Mon. Not. R. Astron. Soc. **332,** 879–890 (2002)

The dual dust chemistries of planetary nebulae with [WCL] central stars

Martin Cohen,[1]★ M. J. Barlow,[2] X.-W. Liu[2] and A. F. Jones[3]
[1]*Radio Astronomy Laboratory, University of California, Berkeley, CA 94720, USA*
[2]*Department of Physics & Astronomy, University College London, Gower Street, London WC1E 6BT*
[3]*Carter Observatory, 40 Salamanca Road, Kelburn, PO Box 2909, Wellington, New Zealand*

Accepted 2002 January 19. Received 2002 January 18; in original form 2001 October 19

ABSTRACT

The rather rare class of central stars of planetary nebulae that show very low-excitation Wolf–Rayet spectra has been a subject of great interest, particularly in the infrared, since its discovery in the late 1960s. Further peculiarities have been found with the advent of infrared spectroscopy from *ISO*. Notably, these objects simultaneously betray the presence of regions of carbon-rich and oxygen-rich dust chemistry. We compare and contrast complete *ISO* spectra between 2 and 200 μm of a sample of six [WC8] to [WC11] central stars, finding many similarities. Among this sample, one star provides strong evidence of quasi-periodic light variations, suggestive of a dust cloud orbiting in a plane from which we view the system.

Key words: astrochemistry – stars: chemically peculiar – circumstellar matter – stars: evolution – stars: Wolf–Rayet – planetary nebulae: general.

1 INTRODUCTION

Our knowledge of BD + 30°3639 ([WC9], hereafter BD) extends back over a century (Campbell 1893) yet the latest type WC stars found as central stars of planetary nebulae (hereafter [WCL]s) were recognized as emission-line objects only in the late 1960s (Henize 1967; Bidelman, MacConnell & Bond 1968; Cowley & Hiltner 1969). Two particularly famous objects, CPD −56°8032 = He 3-1333 (hereafter CPD) and He 2-113 = Hen 1044 (hereafter HE), were classified by extrapolation from known [WC9] central stars of planetary nebulae (CSPNs) as '[WC10]' by Webster & Glass (1974), who also discovered near-infrared excesses in the *JHKL* bands. By 1975, the steeply rising energy distribution of HE from 1 to 20 μm had been measured (Cohen 1975), and that of CPD followed some years later (Cohen & Barlow 1980). Aitken et al. (1980) presented 8–13 μm spectra of CPD and HE, finding both to exhibit strong 11.3- and 8.7-μm polycyclic aromatic hydrocarbon (PAH) features. During the 1990s, intensive *IRAS* follow-on studies led to the discovery of at least one bona fide new [WCL], IRAS 07027–7934 (hereafter 07027), by Menzies & Wolstencroft (1990).

Stratospheric spectroscopy from the *Kuiper Airborne Observatory* (*KAO*) from the 1970s into the 1990s opened up the wavelength region from 5 to 7.5 μm, unavailable from the ground. By this means, Cohen et al. (1989) were able to discover the great strength of the 7.7-μm PAH band in both CPD and HE. Indeed, CPD emits 10 per cent of its total infrared luminosity in this single band, and constitutes the most extreme point in a trend between [integrated 7.7-μm band strength]/*L*(IR) and gas-phase nebular C/O ratio (Cohen et al. 1989) for planetaries in general, not just for [WCL]s. This trend is entirely consistent with the rederivation by De Marco, Barlow & Storey (1997) of these ratios in CPD and HE as 13 and 10, respectively, after careful allowance for the contributions of the stellar wind to the ultraviolet (UV) emission-line fluxes.

Cohen et al. (1999) published the combined Short Wavelength Spectrometer (SWS) and Long Wavelength Spectrometer (LWS) spectrum of CPD and compared it with existing ground-based and *IRAS* photometry. The good agreement, within the uncertainties of these photometric points, between data from the 1970s and 1980s (including *IRAS* LRS and *KAO* spectra) and the *Infrared Space Observatory*[1] (*ISO*: Kessler et al. 1996) spectra suggests the compact nature of the infrared-emitting regions in CPD and HE, as well as the lack of long-term infrared variability. Despite its very strong PAH emission spectrum shortward of 14 μm, Cohen et al. (1999) found strong emission features attributable to crystalline silicates in the *ISO* spectrum of CPD longward of 20 μm. Waters et al. (1998a) found that HE and BD exhibited similar behaviour, with PAHs dominating at $\lambda < 14\,\mu$m and crystalline silicates dominant beyond 20 μm.

2 THE NEBULAE OBSERVED AND THEIR *ISO* SPECTRA

An LWS Consortium programme of observations of [WCL]s was carried out under *ISO* GTO time, supplemented by a small Open Time programme, and sought to obtain both LWS01 and SWS01

[1] Based on observations with *ISO*, an ESA project with instruments funded by ESA Member States (especially the PI countries: France, Germany, the Netherlands and the United Kingdom) and with the participation of ISAS and NASA.

★E-mail: mcohen@astro.berkeley.edu

Table 1. *ISO* SWS and LWS data of [WCL]s that we have utilized.

Object	PNG no.	Spectrum	Instrument	TDT	Date	Speed	Integration (s)
NGC 40	120.0+09.8	[WC8]	LWS01	47300616	03-Mar-1997		1318
NGC 40 off	...	...	LWS01	47300646	03-Mar-1997		1318
NGC 40	120.0+09.8	[WC8]	SWS01	30003803	12-Sep-1996	3	3454
NGC 40	120.0+09.8	[WC8]	SWS01	44401917	02-Feb-1997	2	1912
BD +30°3639	064.7+05.0	[WC9]	LWS01	35501412	06-Nov-1996		1266
BD +30°3639	064.7+05.0	[WC9]	SWS01	35501531	06-Nov-1996	1	1140
BD +30°3639	064.7+05.0	[WC9]	SWS01	86500540	29-Mar-1998	3	3454
CPD −56°8032	332.9−09.9	[WC10]	LWS01	08401538	09-Feb-1996		1552
CPD −56°8032	332.9−09.9	[WC10]	SWS01	13602083	01-Apr-1996	3	3462
CPD −56°8032	332.9−09.9	[WC10]	SWS01	27301339	16-Aug-1996	1	1140
He 2-113	321.0+03.9	[WC10]	LWS01	66900121	14-Sep-1997		2228
He 2-113	321.0+03.9	[WC10]	LWS01	07903229	04-Feb-1996		1554
He 2-113 off	...	...	LWS01	07903253	04-Feb-1996		1554
He 2-113	321.0+03.9	[WC10]	LWS01	60701891	15-Jul-1997		620
He 2-113	321.0+03.9	[WC10]	SWS01	07903307	04-Feb-1996	1	1044
He 2-113	321.0+03.9	[WC10]	SWS01	43400768	23-Jan-1997	2	1912
IRAS 07027−7934	291.3−26.2	[WC10]	LWS01	14101004	06-Apr-1996		1330
IRAS 07027−7934	291.3−26.2	[WC10]	LWS01	56700981	05-Jun-1997		620
IRAS 07027−7934	291.3−26.2	[WC10]	SWS01	14101101	06-Apr-1996	1	1062
IRAS 07027−7934	291.3−26.2	[WC10]	SWS01	73501035	20-Nov-1997	2	1913
K 2-16	352.9+11.4	[WC11]	LWS01	67501340	21-Sep-1997		2230
K 2-16 off	...	...	LWS01	67501357	21-Sep-1997		1329
K 2-16	352.9+11.4	[WC11]	SWS01	29302010	04-Sep-1996	1	1140
K 2-16	352.9+11.4	[WC11]	SWS01	67501241	21-Sep-1997	2	1912

ISO spectra of a subset of the known [WCL]s. We have augmented these spectra by additional material now available through the *ISO* Data Archive. Table 1 summarizes the nebulae observed and the spectra we have found to be useful. This combination of *ISO* data covers almost two orders of magnitude in wavelength space and thereby provides powerful constraints on the overall continua in such nebulae. The SWS Consortium have presented their own SWS spectra of BD and HE (Waters et al. 1998a) but we have again used additional archived *ISO* spectra (Table 1). M 4-18 [WC10] was deemed too faint to attempt an LWS spectrum. Even its SWS data exclude the object from further consideration in this paper because of the noisiness of the data, which leads to major uncertainties in the joining of its subspectra.

Our Consortium LWS01 spectrum of 07027 was lost because of a major solar flare that compromised our data; fortunately, the Data Archive provides two useful LWS spectra of this object, albeit under different, non-*IRAS*, names, 'Vo1' and 'VO-1'. We also include analyses of two nebulae whose spatial extents exceed those of the bright, compact objects (i.e. CPD, HE, BD, 07027) and are comparable to the apertures of the SWS instrument, namely K 2-16 (the sole representative of type [WC11]) and NGC 40 [WC8]. All spectral types given in this paper follow the new classifications by Crowther, De Marco & Barlow (1998). We have omitted IRAS 21282+5050, classified as [WC11] by Cohen & Jones (1987), a type supported by Leuenhagen & Hamann (1998), but now reclassified as O9-9.5 by Crowther et al. (1998). We have also omitted other [WC] nuclei of planetary nebulae (PNe) for which only SWS data exist, such as SwSt 1 (=HD 167362, [WC9pec]) and M 2-43.

The *ISO* SWS01 spectra were generally obtained at Speed 1, although Speeds 2 and even 3 were used for some nebulae. The LWS01 spectra have a resolution of 0.3 μm from 43 to 93 μm, and of 0.6 μm from 84 to 197 μm. All subspectra were spliced together using the same algorithms devised to create absolute, continuous, stellar calibration spectra by Cohen, Walker & Witteborn (1992a). When multiple SWS or LWS spectra were available, these were combined using inverse variance weighting to create single spectra representative of the overall wavelength range of the relevant instrument. When these multiple spectra had different resolutions, the higher were degraded to the resolution of the lower (using appropriate Gaussians) before combining the data. The spliced (individual or combined) SWS spectra were then joined to the spliced LWS, and the complete 2.5–200 μm composites were normalized using *IRAS* data from both the PSC2 and FSS (each recalibrated absolutely: see Cohen et al. 1992b), in all four bands. Both NGC 40 and K 2-16 fill even the largest SWS apertures and the nominal data products for both objects show discontinuities between SWS sub-bands where the apertures change, namely at Bands 3D and 3E. Neither object is optically known to fill the 70-arcsec LWS aperture. Consequently, we have spliced their SWS subspectra by scaling up the data in the shorter-wavelength AOT bands to match those taken through the larger apertures, *before* joining each combined SWS spectrum to the corresponding LWS spectrum. These combined spectra were then normalized to the *IRAS* flux densities.

3 A SET OF WCL SPECTRA

Fig. 1 illustrates the infrared spectra of the four bright [WCL]s in which all nebulae have been simply normalized at their 7.7-μm PAH peaks to the absolute value for CPD at 7.7 μm. K 2-16 does not appear to have PAH emission and is, therefore, omitted from Fig. 1. NGC 40's 11.3-μm feature is dubious but there is a definite 7.7-μm feature. However, the poor signal-to-noise ratio at 7.7 μm renders this an inappropriate wavelength for normalizing the overall spectrum so it too is omitted from Fig. 1 (both these larger

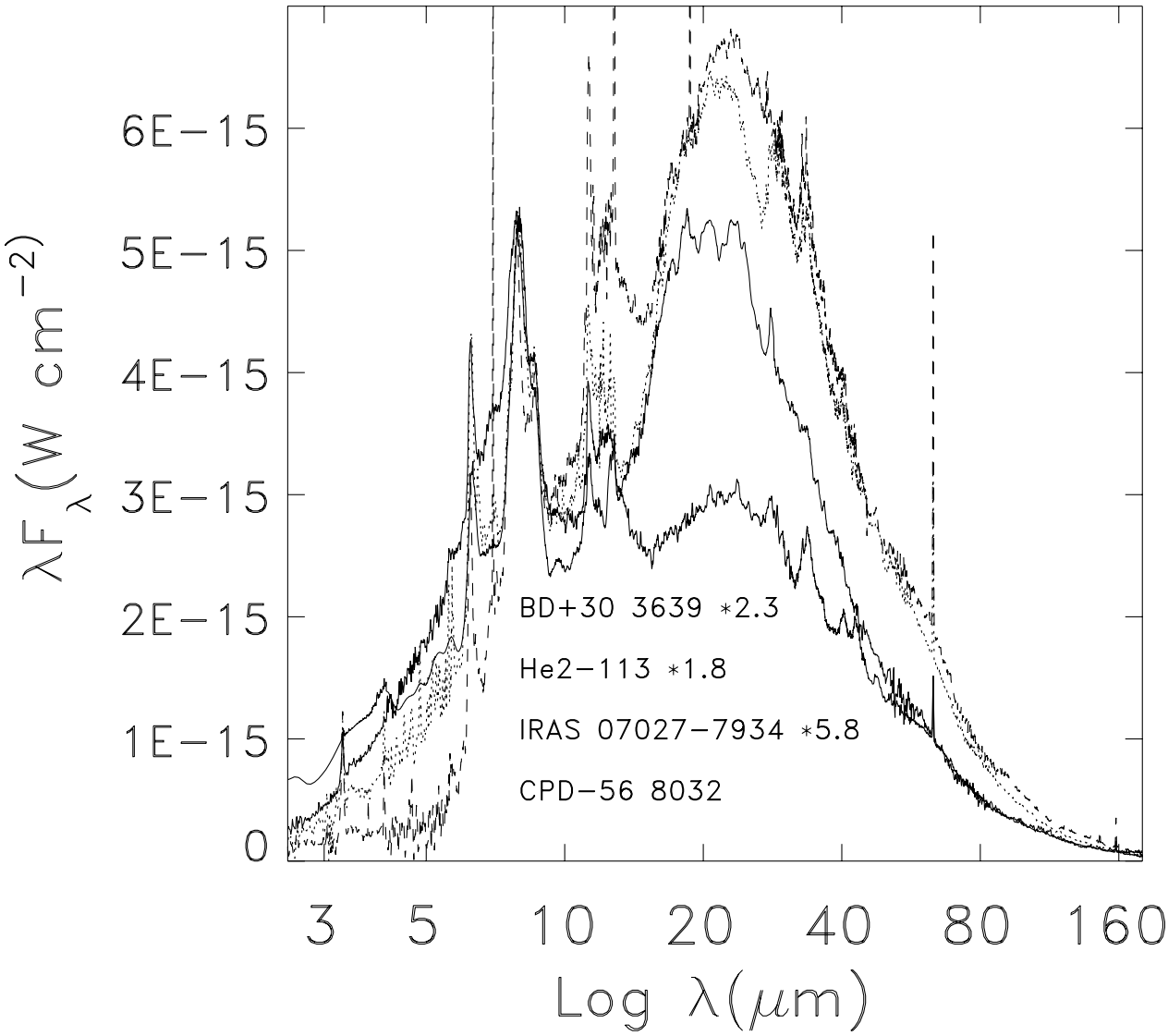

Figure 1. The set of four bright [WCL] spectra. The fluxes of all nebulae have been normalized at their 7.7-μm PAH peaks to the absolute value for CPD. Line styles are: CPD – solid; HE – dots; BD – short dashes; 07027 – dash-dot. Names are indicated in the plot in order of decreasing 20-μm peak strength in the curves.

nebulae are discussed in Section 7). Because of the great strength of PAHs in CPD, this object's long-wavelength spectrum falls below the other spectra, when normalized.

We find this set of overlaid spectra compelling in the sense that it draws attention not just to the crystalline silicate features, that can now be seen as almost a defining characteristic of the [WCL] phenomenon, but to the prominent 'bumps' near 20 and 63 μm. The broad feature near 20 μm most probably represents an amorphous silicate component, for example like those described by Day (1976a,b) or the amorphous pyroxenes presented by Koike et al. (2000).

4 CONTINUUM REMOVAL

Cohen et al. (1999) used the sum of two blackbodies to subtract an assumed underlying featureless continuum of CPD. In this paper, however, the second component is a 'modified blackbody' (i.e. a Planck function multiplied by $\lambda^{-\alpha}$). This method is preferable because use of a second, unmodified, blackbody invariably yields a continuum that exceeds the observed LWS continuum beyond about 100 μm. Modified blackbodies are also physically more relevant to real grain properties than pure blackbodies. However, the primary function of these continua is to provide a means of emphasizing any emission features. In all cases, the complete spectra were inspected by eye to eliminate all previously recognized emission features and a lower-bound algorithm was run to determine the best-fitting continuum for each object using least-squares minimization. The continua were constructed using the sets of parameters returned by this routine (two blackbody temperatures and their scalefactors, and the far-infrared wavelength dependence of grain emissivity), after the lower-bound fits were inspected by eye and adjusted, if deemed necessary, to obtain more satisfactory lower envelope fits to the entire spectral range available.

Fig. 2 illustrates the two components of these continua, and their totals, and compares these with the complete *ISO* spectra of the [WCL]s. Table 2 gives details of the continua used to define the various spectral features in the four bright nebulae. We might have

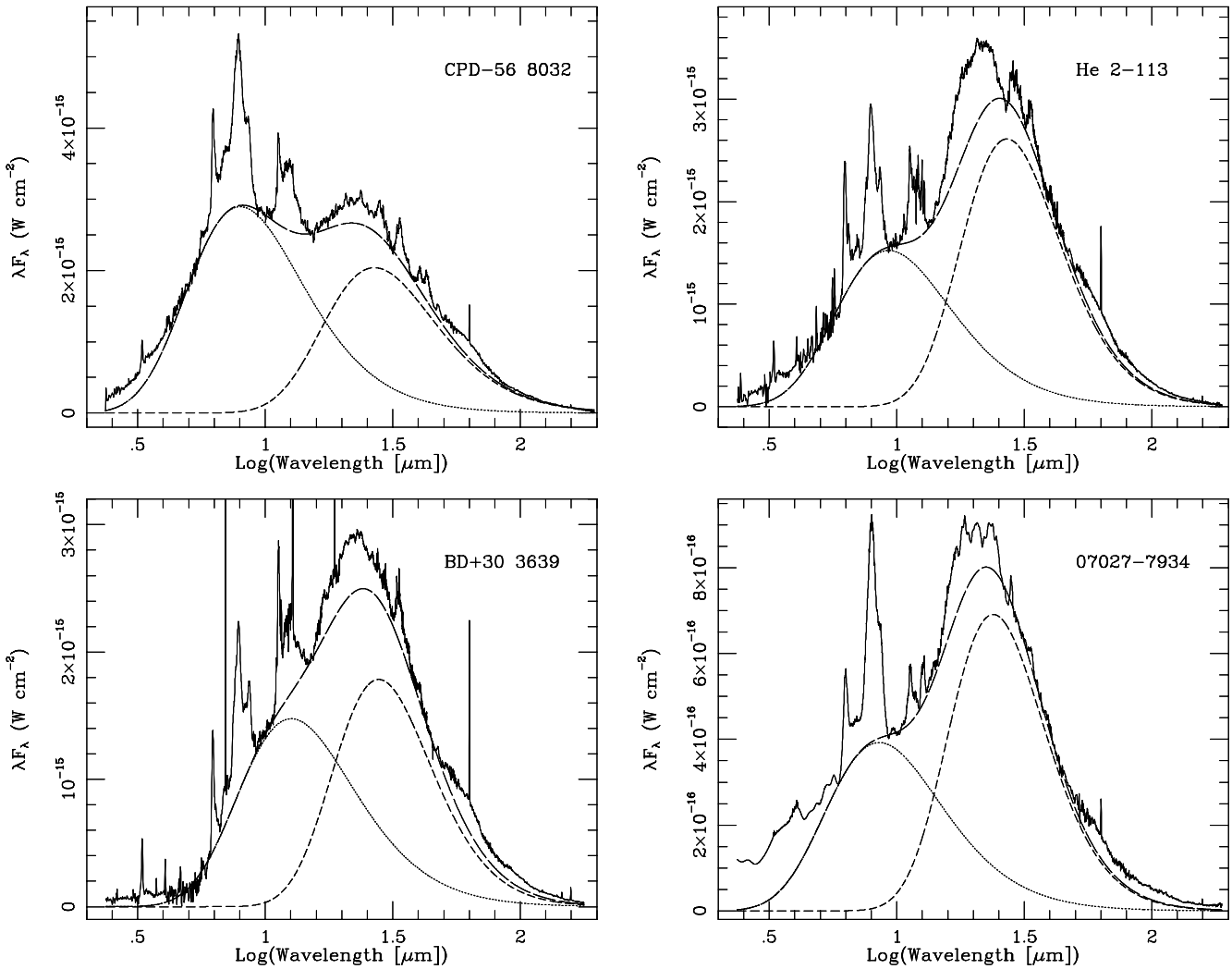

Figure 2. The four bright [WCL] spectra with the adopted continuum elements used to emphasize the emission features, and their totals.

Table 2. Two-component dust continua subtracted from complete [WCL] spectra.

Nebula	Warm BB (K)	Scale (warm)	Cool modified BB (K)	Scale (cool)[a]	α in λ^{α}
NGC 40	...	...	120	1.7e−13	−1.5
BD +30°3639	290	5.0e−17	98	4.2e−13	−1.3
CPD −56°8032	460	1.55e−17	125	1.0e−14	−0.5
He 2-113	395	1.5e−17	103	3.4e−13	−1.2
IRAS 07027−7934	430	2.75e−18	110	1.7e−13	−1.5
K 2-16	265	5.7e−18	115	8.5e−14	−1.5

[a]Scale is the factor applied to the Planck function to fit the spectra.

used two modified blackbodies with a common spectral index, α, but this would lead only to relatively small changes in the inferred temperature of the warmer material, and our primary purpose is simply to remove a plausible continuum from each spectrum to highlight the emission features.

In Section 8 and Fig. 9(a) we investigate the relationship between well-known PAH emission bands in the spectra of our sample of PNe. Because the identification of these features as PAHs and the correlations between these bands have been long established, we can use the recovery of the trends as supporting the general efficacy of our method for interpolating continua when applied to even weaker features. While the detailed shapes of weak bands may depend on the nature of these interpolations, for example, the precise locations of peaks may move at the level of $\sim 0.3\,\mu$m, the integrated band intensities and any identifications in this paper with specific families of materials are robust.

We have made no attempt to match the nebular spectra below $\sim 7\,\mu$m because our emphasis is at longer wavelengths. At these short wavelengths, the contributions of the CSPNs and their stellar winds are falling rapidly with increasing wavelength. Even for CPD, the sum of these additional sources of continuum emission total only about 20 per cent of the flux observed at $3\,\mu$m, and are negligible by $5\,\mu$m. To account for the excesses in these PNe in the $3-5\,\mu$m region, one must appeal to a combination of: thermal

emission from hot, perhaps freshly condensed, dust grains; the plateau of emission underlying the 3.3-μm PAH band attributed to small carbon particles (entities containing hundreds of carbon atoms, distinct from PAH molecules with their tens of carbon atoms); and nebular free–free emission.

Note that, with the exception of CPD, all nebulae require a wavelength dependence of emissivity of the cooler grains close to -1.3, in agreement with the values suggested for amorphous carbon grains in carbon star outflows (Suh 2000). This suggests that even these cooler grains, producing featureless continua, are likely to be a carbon-rich population. The apparent variations in this dependence from object to object are probably insignificant, except for the much smaller index found for CPD. The associated uncertainties are likely to be of order 0.3. Suh (2000) notes that typical laboratory measurements of the far-infrared wavelength dependence for amorphous carbon grains yield values from -0.6 to -1.5, and depend on 'the degree and structure of crystallization' (e.g. Koike et al. 1995). Specifically, these authors found that, for spectral indices less steep than -1, the index depends on the size and number of microcrystallites, with larger size producing steeper dependence. For indices steeper than -1, it is the degree of orientation that matters. Highly oriented (e.g. onion-like layers) materials yield much shallower dependences than plates, whiskers, or truly amorphous materials. Within this context, one might infer that the environment of CPD is unusual in having produced an abundance of very small ($\sim$15 Å) microcrystallites. Speculating, one might further suggest that this means that the far-infrared emitting grains around CPD have not yet suffered much irradiation and annealing by UV photons, both of which processes cause graphitization.

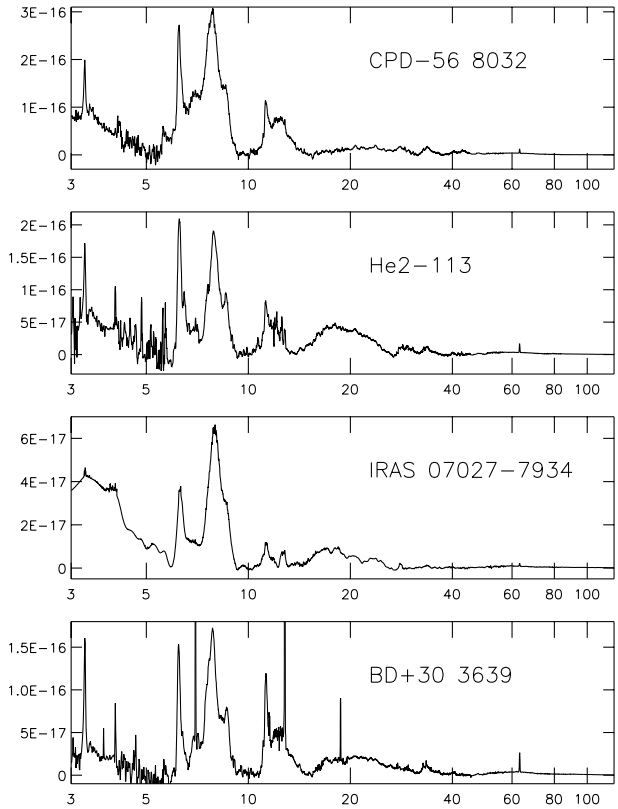

Figure 3. 'Excess spectra' (F_λ, in W cm^{-2} μm^{-1}) of the four brightest [WCL]s for the 3–120 μm region.

5 COMPARISON OF THE EXCESS SPECTRA

Figs 3, 4, 5 and 6 present separate montages of the four bright excess spectra (defined as the difference between the complete observed spectra and the continua specified in Table 2), each covering a spectral range chosen to highlight a particular group of features.

To compare features directly from object to object, Fig. 6 presents appropriately scaled overlays of these four excess spectra for three different spectral regions: 14–26, 25–45 and 40–80 μm. These dramatically show that the 20-μm region, so rich in crystalline silicates in CPD, is overwhelmed by amorphous silicate emission in HE and BD. (Object 07027 appears to have a crystalline emission feature near 18.5 μm but its statistical significance is poor, on the basis of comparison between the two independent SWS spectra and the resulting uncertainties in the formal inverse variance weighted combination of these spectra. The feature is rendered more conspicuous in the excess spectrum by the removal of the bright continuum.) Longward of 28 μm, there is general accord in the appearance of crystalline features in all four objects, although relative strengths vary greatly.

Fig. 6 also shows that, although CPD has strong emission features at 43 and 47.5 μm, these features are much weaker in the spectra of the other objects. Object 07027 also has an exceptionally well-defined 12–14 μm PAH complex, yet in none of our nebulae do we see evidence for the 16.4-μm feature or the underlying 15–20 μm plateau described by van Kerckhoven et al. (2000). These authors attribute this plateau to a blend of many C–C–C bending modes in relatively large PAHs and PAH clusters (with thousands of carbon atoms), and the sharper 16.4-μm band to in-plane C–C–C bending in smaller PAHs (20–100 carbon atoms).

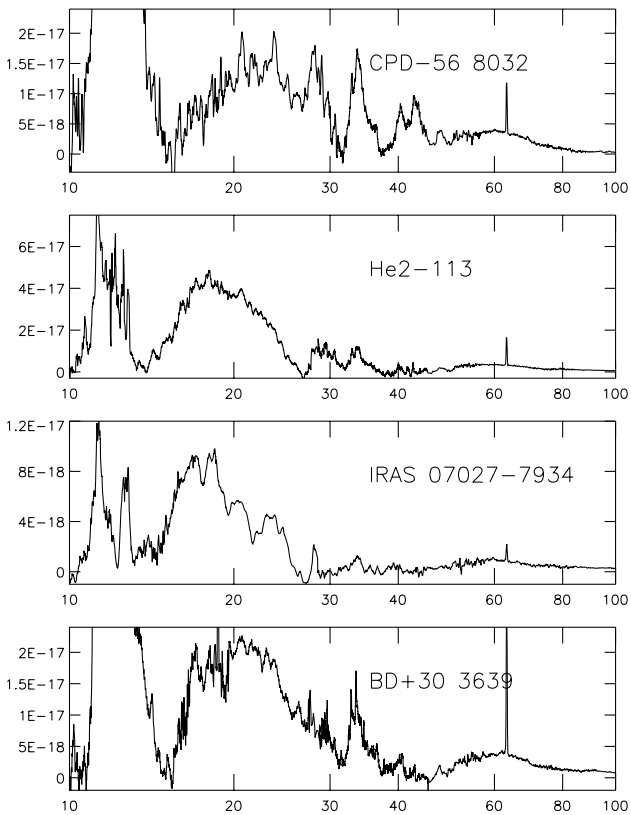

Figure 4. 'Excess spectra' (F_λ, in W cm^{-2} μm^{-1}) of the four brightest [WCL]s for the 10–100 μm region.

The 15–20 μm plateau is thought to be due to the same family of PAHs responsible for the 6–9 μm plateau, so the absence of the former, when the latter is so prominent, in the [WCL]s is puzzling, unless the longer-wavelength plateau is simply hidden by the broad amorphous silicate features.

6 TABULATION OF THE OBVIOUS PEAKS IN THE EXCESS SPECTRA

Table 3 summarizes the wavelengths of the more obvious peaks detectable in the continuum-subtracted excess spectra. Identifications are based on the work of Jager et al. (1998), Koike et al. (2000), Bowey et al. (2001) and Molster et al. (2001). We have assigned peaks to several groupings: enstatite (representing pyroxenes and orthopyroxenes), forsterite (the olivines), crystalline water ice, and the individual clinopyroxene, diopside (because of its likely dominant contribution to the broad feature seen in the [WCL]s near 60 μm). We note that diopside also produces strong features near 25 and 40 μm (Koike et al. 2000; Bowey et al. 2001), the former seen only in BD, the latter in HE, BD and 07027. The remaining features are currently unidentified. Assignments were made if the laboratory and astrophysical wavelengths match within

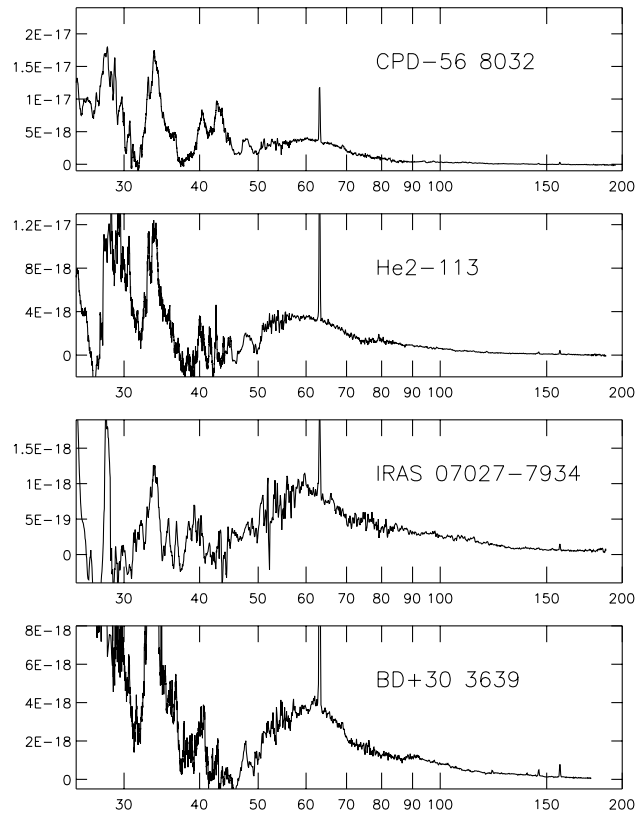

Figure 5. 'Excess spectra' (F_λ, in W cm^{-2} μm^{-1}) of the four brightest [WCL]s for the 25–200 μm region.

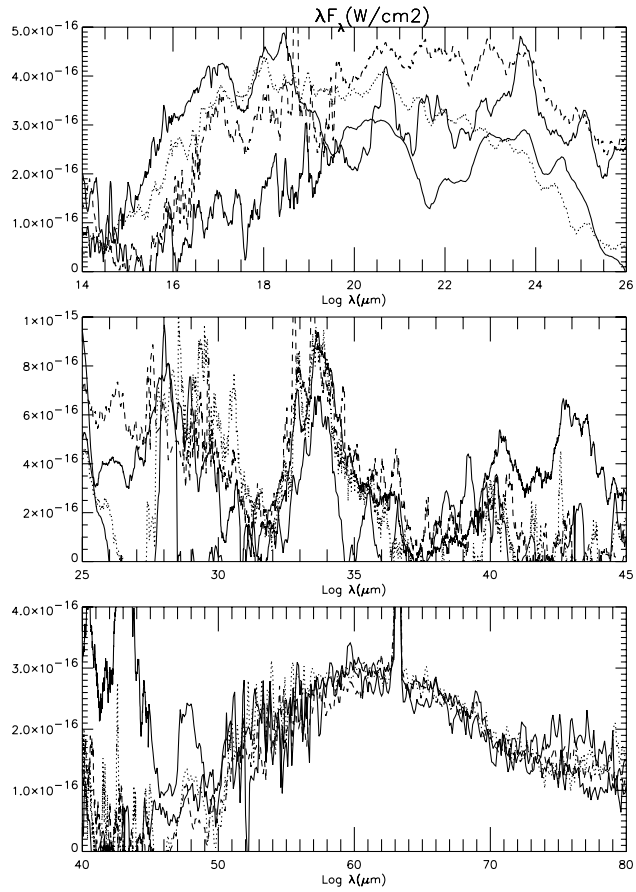

Figure 6. 'Excess spectra' overlaid for the four brightest [WCL]s. Line styles are: CPD – solid; HE – dots; BD – short dashes; 07027 – dash-dot.

Table 3. Peak wavelengths (μm) of probable crystalline dust emission features above the continua in the continuum-subtracted 14–80 μm [WCL] spectra, and suggested identifications.

Nebula	Enstatite	Forsterite	Water ice	Diopside	Unidentified features
CPD −56°8032	20.7, 21.5, 22.8, 22.9, 28.1, 28.9, 29.5, 29.8, 30.7, 35.5, 40.5, 42.7, 43.1, 60:	23.7, 33.8, 69.0	43.5, 60:	60:	25.1, 31.0, 32.0, 32.8, 38.3, 38.7, 39.4, 39.8, 41.7, 47.5, 51.2
He 2-113	18.0, 20.7, 29.5, 29.9, 30.6, 36.2, 40.5, 60:	33.8, 42.6	43.5, 60:	40.1, 60:	32.9, 41.5, 41.7, 41.8, 43.8, 47.5, 79.0
BD +30°3639	22.9, 26.3, 28.0, 29.6, 30.6, 36.5, 40.6, 60:	23.7, 27.6, 33.5, 68.8	43.5, 60:	24.9, 40.2, 60:	17.0, 32.7, 42.8, 47.5
07027−7934	18.0, 18.5, 24.6, 28.0, 29.0, 35.5, 36.6, 40.5	23.7, 33.7, 69.0	43.3, 60:	40.2, 60:	15.8, 17.0, 32.0, 38.3, 39.2, 41.5
K 2-16	20.0, 20.5, 22.7, 24.2, 29.0	23.9, 27.6, 69:		60:	35.8

0.2 μm, although this is of necessity somewhat loose because of variations of peak wavelength with temperature (Bowey et al. 2001) and with crystalline structure (i.e. with clino- or ortho-forms: Koike et al. 2000). The broad bump near 60 μm is denoted by '60:' and it is assigned to each of the enstatite, water ice and diopside columns. CPD is rich in crystalline features while the other nebulae show fewer obvious features. We note that the stronger features in the [WCL]s match the emission peaks in the spectrum of GL 4106, an extreme, dust-shrouded, oxygen-rich asymptotic giant branch (AGB) star (Jager et al. 1998), that of NGC 6302 (Molster et al. 2001), and even that of the Red Rectangle (Waters et al. 1998b), with its peculiar binary.

The dominant sharp features in the spectra of these nebulae can be grouped into the carbon-rich PAH bands that are prevalent below 14 μm, and the oxygen-rich, crystalline silicate bands. The latter have been attributed (e.g. Molster et al. 2001) to the Mg-rich silicates, forsterite and enstatite. Applying this view to the [WCL]s, forsterite would contribute the bands at 23.7, 33.8 and 69 μm, while enstatite contributes those at 28.0, 40.5 and 42.7 μm. Note, however, that it is not uncommon for different portions of an apparently single band to be caused by different kinds of silicate; for example, Waters et al. (1998a) suggest that both olivines and pyroxenes emit near 23 and 33 μm.

7 THE TWO LARGER NEBULAE: NGC 40 AND K 2-16

Fig. 7 shows the rather noisy data for K 2-16, compared with the best-fitting continuum (Table 2), while the second panel illustrates the excess spectrum. The sole LWS spectrum of K 2-16 suffered from a high-temperature detector problem that caused the loss of data beyond about 120 μm (i.e. extra noise afflicted detectors LW3 and beyond, although most of the LW2 subspectrum was usable). Three things are of immediate interest. First, the spectrum of K 2-16 appears to be dominated by a smooth continuum. Secondly, in spite of the noise, there is a broad 60-μm excess emission in its spectrum, very similar in extent to those seen in the spectra of the bright [WCL]s. Thirdly, the [O I] and [C II] emission lines, common in the general interstellar medium and frequently encountered in planetaries even when 'off' position LWS spectra are available for subtraction (Liu et al. 2001), are not seen in the net LWS spectrum of K 2-16.

Fig. 8 illustrates the combined SWS+LWS spectrum for NGC 40, compares it with the best-fitting continuum, and shows the excess over this continuum. A single modified blackbody suffices to provide an adequate fit to this nebula's continuum when one recognizes that the large feature above this component, centred on the 12.8-μm [Ne II] line, is likely to be the broad emission plateau associated with PAHs between about 11 and 15 μm, consistent with the appearance of the 7.7-μm PAH feature. Like K 2-16, NGC 40 may also show a broad emission hump centred near 60 μm although this is not very convincing. The absence of any obvious 20-μm amorphous silicate peak would then be consistent with the lack of any crystalline silicates in this nebula. Hony, Waters & Tielens (2001) have recently identified emission features near 21 and 30 μm in NGC 40 (with central star HD 826) whereas, in our own analysis of the combined SWS spectra of this nebula, we ascribed any structure near these nominal wavelengths to noise.

8 TRENDS AMONG FEATURE STRENGTHS

The purpose of this paper is to demonstrate the strong similarities

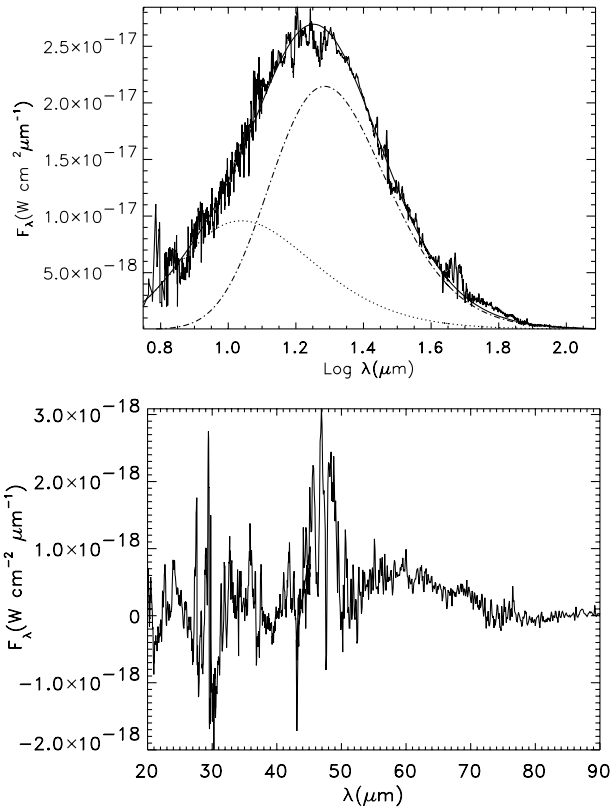

Figure 7. Combined SWS and LWS spectra for K 2-16, showing the adopted best-fitting continuum (top) and excess spectrum (bottom).

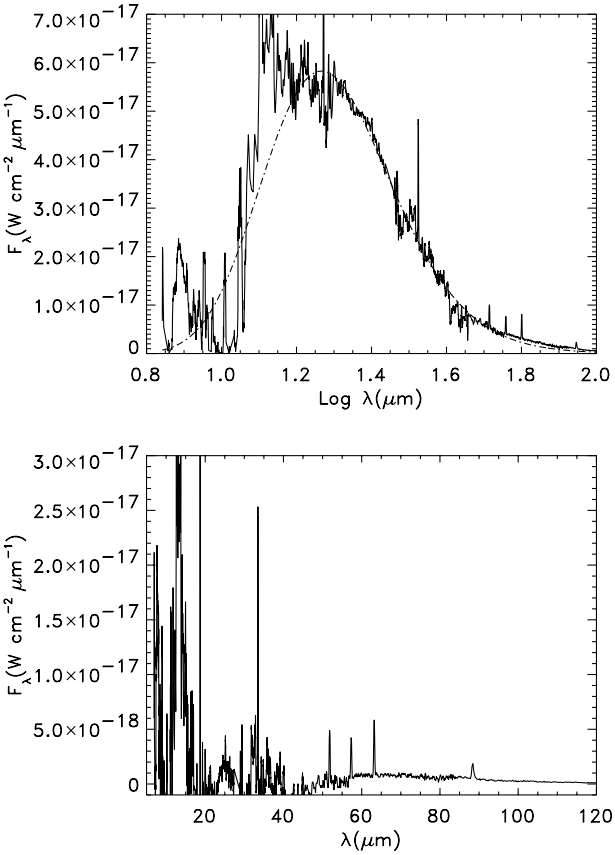

Figure 8. Combined SWS and LWS spectra for NGC 40, showing the adopted best-fitting continuum (top) and excess spectrum (bottom).

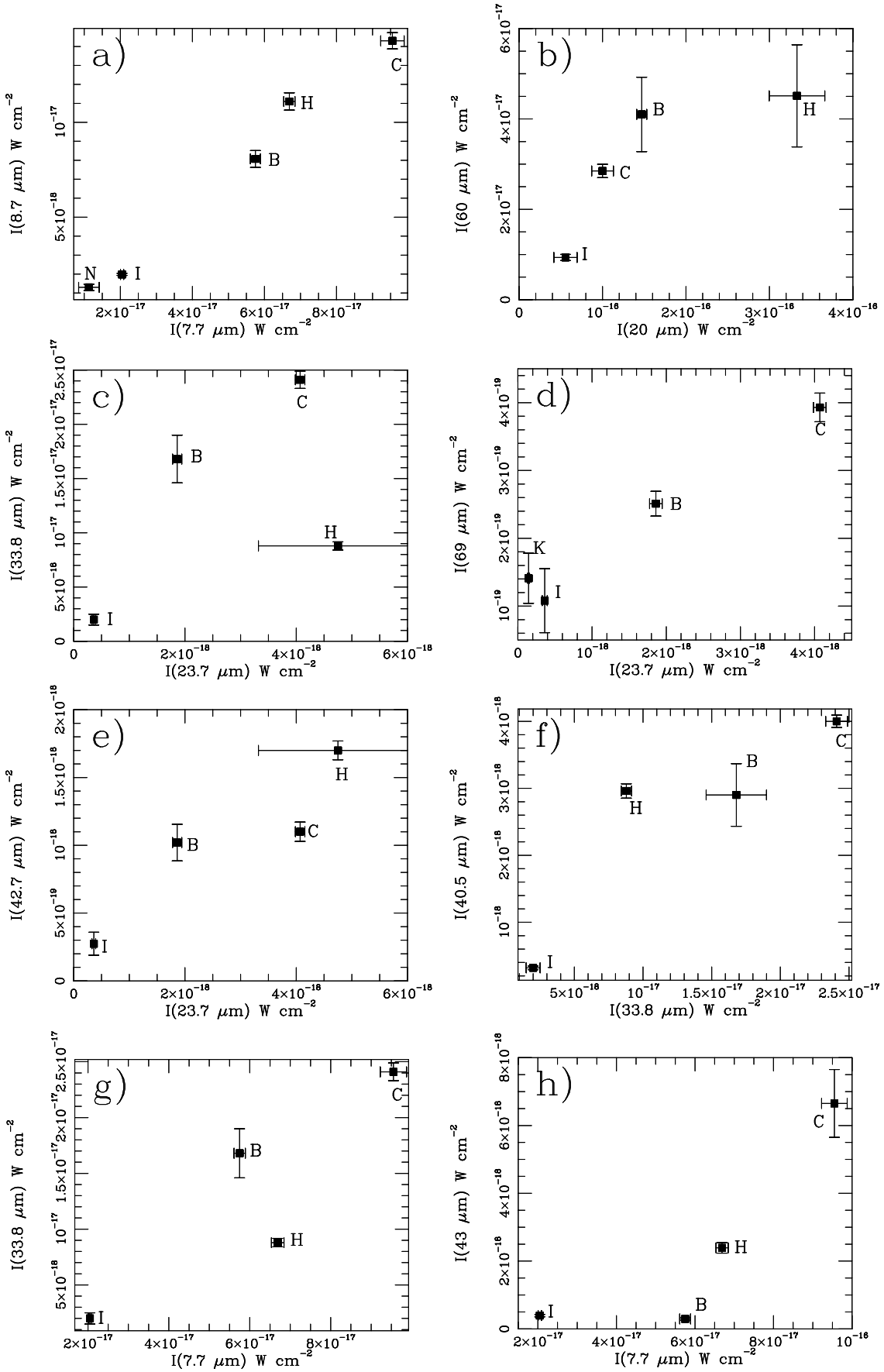

Figure 9. Trends between integrated intensities (W cm^{-2}) of PAH, amorphous and crystalline silicate bands. Nebulae are: C = CPD; H = HE; B = BD; I = 07027; K = K 2-16; N = NGC 40.

in spectral appearance among the [WCL] PN nuclei as a class. To this end, Fig. 9 illustrates eight relationships between different features. Note that the band 'strengths' we use are the integrated intensities ($W\,cm^{-2}$) of the relevant peaks in the excess spectra. The spectrum of the excess emission in CPD was used as a basic template to determine common wavelengths for integration of each feature in other nebulae, although we permitted variations in these wavelengths to accommodate adverse noise in the spectra of specific objects. We plot error bars associated with each PN. These include the estimated uncertainties in the continua that defined the excess spectra, errors that are inherent in the processed SWS spectra, and the formal uncertainties in integrating over these bands. Table 4 summarizes the feature strengths, errors and the full width at half-maximum (FWHM) of these bands in the different PNe. The FWHMs are based solely on the observed spectra without assuming any analytic form for the bands.

To represent the carbon-rich materials, Fig. 9(a) plots two features attributable to PAH emission, namely the 8.7-μm C–H in-plane bending mode and the 7.7-μm C–C stretch. It incorporates integrated band strengths for five PNe (all but K 2-16). Similar trends exist for the 6.2- and 11.3-μm bands in relation to that at 7.7 μm, exactly like those found originally by Cohen et al. (1989). Their absence in K 2-16, which is a rather large nebula exceeding the SWS aperture sizes, may indicate simply that the SWS samples too small a volume of the peripheral photodissociation region when pointed directly at the central star.

For the oxygen-rich grains we offer several comparisons, some of which strengthen the suggested mineral identifications while others are oddly less conclusive. Fig. 9(b) shows the relationship between the broad, amorphous 20-μm feature in these nebulae and the broad 60-μm emission. The three PNe with the weakest 60-μm features show a steep relationship between the two band intensities, but this trend appears to saturate rapidly in HE, where a large increase in 20-μm band strength yields only a small increase in 60-μm intensity. The 60-μm feature (Fig. 5 shows these features more clearly) was attributed to a combination of crystalline water and clinopyroxenes by Cohen et al. (1999). Note that ice contributes no more than about 20 per cent of this integrated feature in CPD and probably less in the other three bright nebulae. In their study of pyroxenes, Koike et al. (2000) present a broad (FWHM ~ 7 μm; full width zero intensity, FWZI ~ 13 μm) feature, peaking at 65.7 μm, in diopside, a calcium-rich crystalline clinopyroxene. The unusual width of this band is well shown by Bowey et al. (2001), who examine the temperature dependence of several olivines and pyroxenes. Direct comparison of the spectrum of diopside with the features observed in the high-excitation PN NGC 6302 by Koike et al. (2000) suggests the relevance of this material to planetaries. The same conclusion was drawn by Molster et al. (2001), in their own analysis of NGG 6302, although they, too, comment on the need for a blend with crystalline water ice and enstatite (another pyroxene) to satisfy the width of this feature. One can interpret this trend as confirming the suggestion (e.g. Molster & Bradley 2001) that crystalline silicates in PNe are derived from the annealing of amorphous silicates so that, until exhaustion of the reservoir of amorphous materials, the quantities of crystalline and amorphous silicates are proportional.

If the specific attributions of Molster et al. (2001) were correct, one would expect correlations between the bands at 33.8 and 23.7 μm, and between those at 69 and 23.7 μm. Fig. 9(c) plots the putative forsterite bands at 23.7 and 33.8 μm. The strength of the 33.8-μm feature in HE is very low, weakening any trend in this diagram, although the remaining three PNe show a significant correlation.

According to the work of Koike, Shibai & Tuchiyama (1993), the weak 69-μm band is a feature of very pure forsterite and we find it to be well correlated with the 23.7-μm band intensity (Fig. 9d) in the four objects that show the 69-μm feature. Bowey et al. (2001) have discussed the temperature dependence of observable parameters of the 69-μm forsterite band, namely the shifting to shorter wavelengths of its peak wavelength with decreasing temperature, together with a narrowing of its FWHM.

In Figs 9(e) and (f), we explore two mixed relationships by plotting the 42.7-μm enstatite against the 23.7-μm forsterite band, and the 40.5-μm enstatite against the 23.7-μm band, respectively. These produce acceptable correlations, perhaps reinforcing the point that, until this field has advanced to the point of definite mineral identifications for all these bands, we must acknowledge the simultaneous contributions of more than one crystalline silicate component to several of the observed bands. Note that our '40.5-μm' bandstrength is an integration between ~ 39.5 and 41.2 μm, and includes dominantly the enstatite peak near 40.5–40.6 μm, as well as any subsidiary peak attributable to diopside, close to 40.0 or 40.1 μm.

Table 4. Band strengths in Fig. 9 for the [WCL] PNe, in units of $10^{-20}\,W\,cm^{-2}$, with estimated uncertainties in parentheses, together with the FWHM of each band in μm (on the second line for each object).

Nebula	7.7 μm	8.7 μm	20 μm	23.7 μm	33.8 μm	40.5 μm	42.7 μm	43 μm	69 μm	60 μm
CPD	9600(320)	1400(44)	10000(1300)	410(9)	2400(80)	400(9)	110(7)	670(100)	39(2)	2850(150)
	0.55	0.27	5:	0.43	1.63	0.93	0.46	1.37	0.60	10
HE	6700(150)	1100(46)	33000(3300)	480(140)	880(38)	300(11)	170(7)	240(15)	...	4500(1100)
	0.42	0.20	7.1	0.75	1.33	0.84	0.16	0.20	...	14
BD	5800(140)	810(44)	15000(600)	190(8)	1700(220)	290(47)	100(14)	30(4)	25(2)	4100(820)
	0.48	0.23	6.2	0.70	1.01	0.93	0.53	0.48	0.50	14
07027	2100(43)	200(5)	5600(1400)	36(3)	200(50)	32(3)	27(8)	39(3)	11(4.5)	940(67)
	0.52	0.24	8.4	0.41	1.08	0.87	0.13	0.77	0.50	14
K 2-16	38(3)	...	...	14(2)	...	...	...	...	14(4)	...
	0.1:	...	...	0.44	...	...	...	...	0.2:	13
NGC 40	1100(290)	1300(17)	...	...	...	370(8)	69(2)	...	...	490(21)
	0.60	0.19	...	...	...	0.72	0.48	...	...	14

Finally, in Figs 9(g) and (h), we show two more hybrid trends, comparing first the 33.8-μm crystalline silicate band, and secondly the 43-μm ice + silicate feature, with the 7.7-μm PAH strength. Each yields an acceptable relationship for the bright [WCL]s although the interpretation of this relationship is obscure.

The existence of the various relationships between observed band intensities might be taken as proof that each of these [WCL]s is similar in the presence of crystalline silicates, amorphous silicates and a PAH-emitting inner zone. In such a picture, the trends could result simply from a common phenomenon in PNe with similar progenitor masses, that are viewed at different distances from the sun. However, if not merely fortuitous, Figs 9(g) and (h) might also imply that the recent strength of carbon-rich mass loss from these nuclei is somehow related to the amount of crystalline silicates formed in the preceding evolutionary phase.

We can arrange the four bright [WCL] CSPNs into a sequence that reflects the diminishing strength of the 20-μm amorphous silicate band with respect to the growing strength of the crystalline components. To create such a sequence we have added together the intensities of the dominant crystalline bands (those at 23.7, 28.1, 33.8, near 40.3, 42.7 and 69 μm), and ratioed this sum to the integrated strength of the 20-μm amorphous feature. Using this ratio as an index of crystallinity we find this sequence, in order of decreasing crystalline content of the spectrum, to be: CPD (39 per cent), BD (18 per cent), HE (9 per cent) and 07027 (8 per cent).

We have not yet been able to enlarge the sample of [WCL] PNe presented in Fig. 9. NGC 6302, which also shows PAHs and crystalline features, has no obvious relation to the [WCL] PNe and, while SwSt 1 and M 2-43 are related to the [WCL]s, they have no detectable crystalline silicate features (and very weak or absent PAH emission).

9 THE SPATIAL DISTRIBUTION AND CHARACTER OF THE DUST IN [WCL]s

Cohen et al. (1999) discussed a number of hypotheses that might explain the simultaneous existence of C- and O-rich particles around evolved C-rich objects such as CPD. The main objection to the hypothesis that these objects have experienced a recent thermal pulse, which has converted an outflow that was formerly O-rich into one that is C-rich, is that such a transition should occupy a negligible fraction of the AGB/post-AGB lifetime of a star, whereas many examples of joint O-rich/C-rich dust chemistry are known, including most PNe with [WCL] central stars. The second hypothesis discussed was that one of the grain components (most likely the silicates) is in orbit around the system and existed well before the current evolutionary phase. Two scenarios were explored, one where the orbiting material is in a disc associated with a binary system and the other where the orbiting material resides in a Kuiper belt-like ring left over from the original star formation process.

Intriguing information on the long-term optical variability of CPD has been presented by Jones et al. (1999), who covered a 10-year span, including the first 'R CrB-like decline' announced by Pollacco et al. (1992). Fig. 10 offers a longer-term perspective on the photometric variations of CPD, extending the work of Jones et al. (1999) into 2002. There is now clear evidence for *three* such dimmings of CPD, with a rough pseudo-period of 5 yr, in addition to a slow overall decline. Indeed, by late 2001, CPD was emerging from its most recent event.

Jones et al. also monitored HE. Fig. 11 extends the search for variations in HE into 2002. HE may have shown possible variations in the early 1990s, amounting to perhaps two minima, but no other [WCL] monitored has exhibited any episodes of dimming like those of CPD.

Jeffery (1995) analysed several hot, H-deficient, C-rich stars (including a number of R CrB stars), seeking differences between the derived ultraviolet extinction curves and the normal interstellar law. He sought to explain such differences in terms of circumstellar dust around the stars. CPD was in his sample but, because of the signal-to-noise ratio (S/N) limitations of the *IUE* data, the case for an anomalous circumstellar extinction component was far more subtle than the obviously anomalous circumnebular extinction law towards A30 (see also Greenstein 1981), a born-again PN [i.e. one whose central star has suffered a delayed thermal pulse that has rejuvenated the CSPN and returned it to the beginning of its post-AGB transition across the Hertzsprung–Russell (HR) diagram; see Iben et al. 1983]. Clumps of circumstellar dust can arise when dense gas regions cool, creating condensation nuclei. If one treats BD as a paradigm for later-type [WCL]s, then there is substantive evidence for clumpiness in its wind (in the form of the variability on time-scales of hours and days of small emission components of C III and C IV lines in the optical: Acker, Grosdidier & Durand

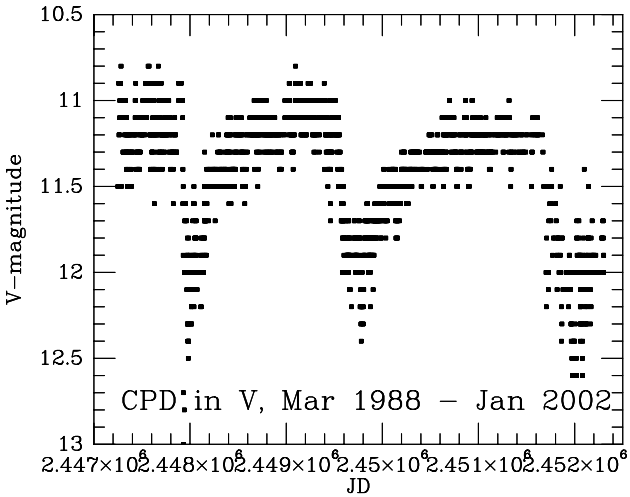

Figure 10. Thirteen years of photometry for CPD −56°8032, showing the three dimmings.

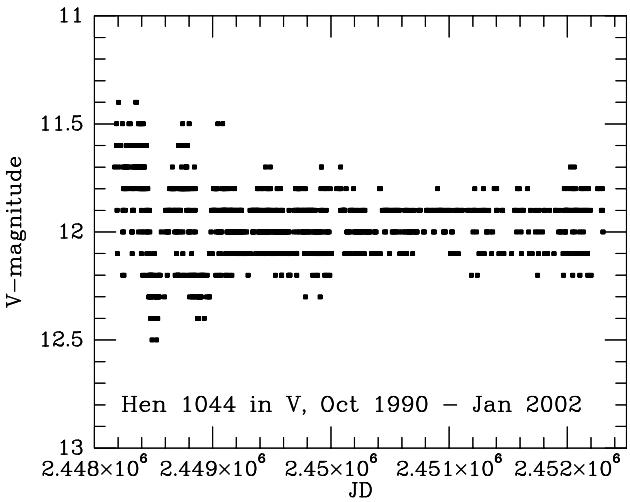

Figure 11. Photometry for He 2-113 (=Hen 1044) over eleven years.

1997), in its dust (comparing *HST* Balmer line and radio continuum maps: Harrington et al. 1997; Bryce et al. 1997), and in the existence of high-velocity molecular knots (Bachiller et al. 2000). Therefore, one is tempted to postulate the existence in other [WCL]s of dusty blobs with much larger than typical nebular extinction, similar to those found around BD (see fig. 7 of Harrington et al. 1997).

High-resolution Hβ imaging of CPD and HE with *HST*/WFPC (De Marco et al. 1997; Sahai, Nyman & Wooten 2000) directly probes their inner structure. In CPD, WFPC imagery reveals a complex set of blobs embedded in more extended nebulosity, redolent of NGC 7027, probably indicative of dense overlying circumstellar dust regions. HE appears very similar, with a mixture of multiple components of bright and faint nebulosity, overlaid by obscuring dust lanes (Sahai et al. 2000). In neither object is there clear evidence that the dust lies in a disc. However, Sahai et al. (2000) have interpreted HE as a bipolar nebula whose central star is offset from any geometric centre, akin to MyCn 18 (Sahai et al. 1999), most probably caused by a binary central star. The link between binarity and bipolar nebulae is circumstantial though suggestive (Cohen 1983), just as Waters et al. (1998b) have argued indirectly that the crystalline silicates around BD and HE must lie in a circumstellar disc, by analogy with other, non-[WCL], systems established as binaries that show crystalline silicates. Several observers have proposed that high-resolution, narrow-band imaging of nebulae from the ground using large telescopes might settle empirically where the crystalline silicate bands and other features arise in PNe. However, this is a difficult experiment from the ground because the best crystalline features occur in regions of poor terrestrial atmospheric transmission, for example those at 23.7 and 28.1 μm.

It is possible to interpret CPD's recent optical dimmings as being caused by either (a) dust condensation events, similar to those exhibited by H-deficient R CrB stars, or (b) some of CPD's circumstellar material being located in a rotating disc- or ring-like structure, in which there is at least one dusty clump that our line of sight happens to have intercepted. We favour option (b) because, although CPD's optical photometric dimmings bear some resemblance to R CrB-like events, the apparent periodicity and lack of extended minima sets them apart from most R CrB dust formation episodes.

A hybrid version of (a) and (b) is known to occur for a number of massive WCL Wolf–Rayet (WR) systems, in which episodic dust formation occurs during the interaction between the wind of a WCL star and that of a binary companion (Williams 1997), producing a spiral-shaped wake of newly formed dust (see the near-infrared interferometric images of WR104 published by Tuthill, Monnier & Danchi 1999). The details of how condensation nuclei might form around even Population I WC stars are still unknown but, granted that they can do so in an equatorial disc around a single WC star (Cherchneff & Tielens 1995), Zubko (1998) describes the physics of 'implantation' of carbon atoms in an outflowing, ionized stellar wind, which promotes the growth of these nuclei. In the case of planetary nebulae with [WCL] central stars, any binary companion is unlikely to have a significant stellar wind of its own, but the interaction of a [WCL] wind with a circumstellar disc around a companion star that was itself in a highly non-circular orbit around the WR star could generate compression effects and episodes of dust formation that would be capable of producing periodic occultations of the WR star, when viewed at a favourable angle. For the [WCL] stars it is premature to attempt to define the physics of such dust-forming events when the basic scenario is so ill-defined.

However, the presence or absence of infrared variability could distinguish between models for CPD's variability that invoke dust formation events and models that invoke occultations by clumpy material orbiting at much larger distances. For example, millimetre-wave interferometric imaging of the dust around Vega, an archetype of the class of main-sequence star exhibiting far-infrared circumstellar dust emission, shows a 95-au radius circumstellar ring that is highly clumped (Koerner, Sargent & Ostroff 2001). Clumped rings of this size or larger might be capable of producing occultation events when viewed from a favourable angle, and precessional periodicity of a dense cloud, or multiple dense clumps, might cause the quasi-periodicity seen in CPD. In such a situation, one would expect no infrared variations to occur during dimmings of the star. If, however, an R CrB-type episode or an interacting-wind dust formation event were responsible for the faintening of CPD, then infrared variations are predicted.

There is no evidence as yet for CPD showing any infrared dust emission variability of the type normally associated with dust formation events. The published literature contains too few measurements of CPD to reveal any meaningful sense of variability and, to our knowledge, no-one has monitored any of the optical dimming episodes of CPD in the infrared. Nonetheless, we note that all three *ISO* spectra of CPD in Table 1 occurred on the recovery from the visual minimum of the second dimming shown in Fig. 10, about halfway between minimum ($V \sim 12.3$) and the locally interpolated value between events ($V \sim 11.0$).

Cohen et al. (1999) suggested that the crystalline silicates and ice particles found around the C-rich central star of CPD could reside in a pre-existing belt or cloud of comets. Since then, Melnick et al. (2001) have discovered circumstellar water vapour around the archetypal carbon star IRC +10216 and invoked a similar explanation, namely the evaporation of orbiting icy bodies during the large luminosity increase accompanying the star's AGB evolution. Saavik Ford & Neufeld (2001) have further explored theoretically the specific case of a C-rich AGB star whose continued mass loss has driven icy bodies outwards, past the classical Kuiper belt zone. Consequently, there could still be icy bodies at large radii that would not suffer complete evaporation at the TP-AGB phase, lending credibility to an origin of the crystalline silicates in a comet cloud.

The apparent change in CPD's period with time emphasizes that no simplistic morphology will suffice. Either the orbital distance of the obscuring dusty region is steadily increasing with time or else we are viewing clumps that are rather regularly spaced around a portion of a large ring. The slow trend toward fainter magnitudes at maximum for CPD could indicate that we are viewing through an increasingly dense region of such a ring. By contrast, the absence of photometric variations in HE indicates that, if this nebula truly contains a dust disc or ring, we do not lie in or close to its plane.

10 CONCLUSIONS

A good working hypothesis seems to be the statement that all [WCL]s showing strong PAHs also show crystalline silicates in emission in their *ISO* spectra. We have arranged the four bright [WCL] CSPNs into a single sequence expressed by our index of crystallinity, that measures the ratio of the total of the major crystalline bands to the 20-μm amorphous silicate feature. This varies from 39 per cent for CPD to only 8 per cent for 07027. Nevertheless, we lack any direct indication of the geometrical organization of either crystalline or amorphous dust components in

these nebulae as a class. Circumstellar clumps of dust appear consistent with a variety of observations of the latest [WCL] types ($\geq$[WC9]). For HE, there is indirect, model-dependent, inference for a flattened organization of nebular material (Sahai et al. 2000). Only for CPD, in which three periodic episodes of stellar dimming are now known, might one suggest that the organization of circumstellar material is most probably disc-like and that the existence of the crystalline silicates might in some way be related to this geometry. The possibility that the observed crystalline silicates reside in a belt or cloud of comets orbiting at large distances from the central star is still open, particularly in view of the recent discovery of water vapour around the AGB carbon star IRC +10216. However, taking all the available evidence into account, we believe that our recent observation of yet another photometric decline in CPD is directly indicative of some kind of binary, with orbital period $\sim$5 yr, associated with a circumbinary disc close to whose plane we lie.

ACKNOWLEDGMENTS

MC thanks NASA for supporting this work through grants NAG5-4884 and JPL961501 with Berkeley, and University College London for hosting him as a short-term visitor on several occasions. We thank Rens Waters and his colleagues for organizing a very fruitful workshop on this topic in Amsterdam in 1999 September, and Janet Bowey for helpful discussions.

REFERENCES

Acker A., Grosdidier Y., Durand S., 1997, A&A, 317, L51
Aitken D. K., Barlow M. J., Roche P. F., Spenser P. M., 1980, MNRAS, 192, 679
Bachiller R., Forveille T., Huggins P. J., Cox P., Maillard J. P., 2000, A&A, 353, L5
Bidelman W. P., MacConnell D. J., Bond H. E., 1968, IAU Circ. 2089
Bowey J. E., Lee C., Tucker C., Hofmeister A. M., Ade P. A. R., Barlow M. J., 2001, MNRAS, 325, 886
Bryce M., Pedlar A., Muxlow T., Thomasson P., Mellema G., 1997, MNRAS, 284, 815
Campbell W. W., 1893, PASP, 5, 204
Cherchneff I., Tielens A. G. G. M., 1995, in van der Hucht K. A., Williams P. M., eds, Proc. IAU Symp. 163, Wolf–Rayet Stars: Binaries, Colliding Winds, Evolution. Kluwer, Dordrecht, p. 346
Cohen M., 1975, MNRAS, 173, 489
Cohen M., 1983, in Flower D. R., ed., Proc. IAU Symp. 103, Planetary Nebulae. Reidel, Dordrecht, p. 45
Cohen M., Barlow M. J., 1980, ApJ, 238, 585
Cohen M., Jones B. F., 1987, ApJ, 321, L151
Cohen M., Tielens A. G. G. M., Bregman J., Witteborn F. C., Rank D. M., Allamandola L. J., Wooden D. H., Jourdain de Muizon M, 1989, ApJ, 341, 246
Cohen M., Walker R. G., Witteborn F. C., 1992a, AJ, 104, 2030
Cohen M., Walker R. G., Barlow M. J., Deacon J. R., 1992b, AJ, 104, 1650
Cohen M., Barlow M. J., Sylvester R. J., Liu X.-W., Cox P., Lim T., Schmitt B., Speck A. K., 1999, ApJ, 513, L135
Cowley A. P., Hiltner W. A., 1969, A&A, 3, 372
Crowther P. A., De Marco O., Barlow M. J., 1998, MNRAS, 296, 367
Day K. L., 1976a, ApJ, 203, L99
Day K. L., 1976b, ApJ, 210, 614
De Marco O., Barlow M. J., Storey P. J., 1997, MNRAS, 292, 86
Greenstein J., 1981, ApJ, 245, 124
Harrington J. P., Lame N. J., White S. M., Borkowski K. J., 1997, AJ, 113, 2147
Henize K. G., 1967, ApJS, 14, 125
Hony S., Waters L. B. F. M., Tielens A. G. G. M., 2001, A&A, 378, L41
Iben I., Jr, Kaler J. B., Truran J. W., Renzini A., 1983, ApJ, 264, 605
Jager C. et al., 1998, A&A, 339, 904
Jeffery C. S., 1995, A&A, 299, 135
Jones A., Lawson W., De Marco O., Kilkenny D., van Wyk F., Roberts G., 1999, Observatory, 119, 76
Kessler M. F. et al., 1996, A&A, 315, L27
Koerner D. W., Sargent A. I., Ostroff N. A., 2001, ApJ, 560, L181
Koike C., Shibai H., Tuchiyama A., 1993, MNRAS, 264, 654
Koike C. et al., 1995, ApJ, 446, 902
Koike C. et al., 2000, A&A, 363, 1115
Leuenhagen U., Hamann W.-R., 1998, A&A, 330, 265
Liu X.-W. et al., 2001, MNRAS, 323, 343
Melnick G. J., Neufeld D. A., Saavik Ford K. E., Hollenbach D. J., Ashby M. L. N., 2001, Nat, 412, 160
Menzies J. W., Wolstencroft R. D., 1990, MNRAS, 247, 177
Molster F. J., Bradley J. P., 2001, Meteorites Planet. Sci., 36, A140
Molster F. J. et al., 2001, A&A, 372, 165
Pollacco D. L., Kilkenny D., Marang F., van Wyk F., Roberts G., 1992, MNRAS, 256, 669
Saavik Ford K. E., Neufeld D. A., 2001, ApJ, 557, L113
Sahai R. et al., 1999, AJ, 118, 468
Sahai R., Nyman L.-A., Wooten A., 2000, ApJ, 543, 800
Suh K.-W., 2000, MNRAS, 315, 740
Tuthill P. G., Monnier J. D., Danchi W. C., 1999, Nat, 398, 487
van Kerckhoven C. et al., 2000, A&A, 357, 1013
Waters L. B. F. M. et al., 1998a, A&A, 331, L61
Waters L. B. F. M. et al., 1998b, Nat, 391, 868
Webster B. L., Glass I. S., 1974, MNRAS, 166, 491
Williams P. M., 1997, Ap&SS, 251, 321
Zubko V., 1998, MNRAS, 295, 109

This paper has been typeset from a TEX/LATEX file prepared by the author.